Flexural behavior of RC beams strengthened with steel–FRCM composite

Article *in* Engineering Structures · November 2016

DOI: 10.1016/j.engstruct.2016.09.006

CITATIONS
64

READS
717

4 authors:

L. H. Sneed
Missouri University of Science and Technology
135 PUBLICATIONS **1,625** CITATIONS
SEE PROFILE

Salvatore Verre
Università della Calabria
24 PUBLICATIONS **293** CITATIONS
SEE PROFILE

Christian Carloni
Case Western Reserve University
121 PUBLICATIONS **1,917** CITATIONS
SEE PROFILE

Luciano Ombres
Università della Calabria
65 PUBLICATIONS **1,305** CITATIONS
SEE PROFILE

Engineering Structures 127 (2016) 686–699

Contents lists available at ScienceDirect

Engineering Structures

journal homepage: www.elsevier.com/locate/engstruct

Flexural behavior of RC beams strengthened with steel-FRCM composite

Lesley H. Sneed [a,*], Salvatore Verre [b], Christian Carloni [c], Luciano Ombres [b]

[a] Department of Civil, Architectural and Environmental Engineering, Missouri University of Science and Technology, Rolla, MO, USA
[b] Department of Civil Engineering, University of Calabria, Cosenza, Italy
[c] Department of Civil, Chemical, Environmental, and Materials Engineering, University of Bologna, Bologna, Italy

ARTICLE INFO

Article history:
Received 25 May 2016
Revised 6 August 2016
Accepted 8 September 2016

Keywords:
Bond
Direct-shear test
Fiber strain
Flexural strengthening
Steel-FRCM composite

ABSTRACT

This paper presents the results of an experimental investigation of the flexural response of reinforced concrete (RC) beams strengthened using externally bonded steel fiber reinforced cementitious matrix (steel-FRCM) composite. Steel-FRCM composite strips were bonded to the tension face of four RC beams, which were tested in four-point bending. Parameters varied were the presence/absence of the external (coating) layer of the matrix, presence/absence of U-wrap anchorages, and loading rate. Results are compared with those from single-lap direct-shear tests conducted on the same composite. The direct-shear tests showed that debonding of steel-FRCM joints is characterized by fiber slippage and fracture of the matrix layer at the internal matrix layer-fiber interface. In the beam tests, the strengthening system increased the yield load by 15–21% relative to the unstrengthened beam. The ratio of the load at which debonding occurred to the load at yielding ranged from 1.11 to 1.19 for each strengthened beam. The load rates employed and the presence of the external matrix layer did not appear to significantly affect the failure mode or the load and midspan displacement at debonding. The presence of the U-wraps helped restrain the peel-off of the composite observed in strengthened beams without the U-wrap, however, they did not restrain the fiber slippage at the ends of the composite, which inhibited composite action. Average values of the maximum fiber strain at composite debonding determined using strain profiles from strain gages, an approximate method, and moment-curvature analysis were 0.54%, 0.73%, and 0.83%, respectively.

1. Introduction

Fiber reinforced composites have been widely used to strengthen reinforced concrete (RC) members since they have a high strength-to-weight ratio, require relatively limited time to cure, and have mechanical properties that can be engineered to meet the desired structural performance. Fiber-reinforced polymer (FRP) composites, which are comprised of continuous fibers (usually carbon, glass, or aramid) and a thermosetting (organic) resin, are currently the most common type of composite system used for structural strengthening applications. Another type of composite that was recently developed is referred to as fiber reinforced cementitious matrix (FRCM) composite, which contains continuous fibers with a cementitious (inorganic) matrix. The use of inorganic matrix was proposed to address some of the inherent disadvantages associated with the use of organic resin in FRP composites, such as lack of moisture vapor transmission [1].

A new class of composites that is being explored includes steel fiber sheets with either an inorganic matrix or an organic matrix described above. The use of steel fibers was proposed as a lower-cost alternative to other fiber types used in FRCM or FRP composites such as carbon, aramid, glass, or polyparaphenylene benzobisoxazole (PBO). The resulting composites have been referred to in the recent literature by different names, but are herein referred to as steel-FRCM and steel-FRP, respectively. Published literature on steel-FRCM and/or steel-FRP composites dates from 2004 [2,3]. Different authors have studied the use of steel-FRCM and/or steel-FRP for flexural strengthening of RC beams [2–11] and RC slabs [12]. These studies have shown that steel-FRCM and steel-FRP composites are effective in increasing the flexural strength of the member, although debonding of the composite tends to limit the effectiveness except in cases of relatively low fiber density where fiber rupture has been observed [12]. Experimental evidence in the literature reports that debonding of steel-FRCM composite can occur within the composite [12] instead of within a thin matrix-rich layer of the concrete substrate as is typically the case with FRP composites [1]. Interestingly, the limited number of studies that have investigated mechanical anchorage

* Corresponding author.
E-mail addresses: sneedlh@mst.edu (L.H. Sneed), salvatore.verre@unical.it (S. Verre), christian.carloni@unibo.it (C. Carloni), luciano.ombres@unical.it (L. Ombres).

http://dx.doi.org/10.1016/j.engstruct.2016.09.006
0141-0296/

of steel-FRCM composites have shown that anchorage did not significantly improve the performance of the strengthening system [3,7,13]. Therefore, for design purposes it is important to understand the debonding process and potential factors that may help mitigate this mode of failure.

This paper presents the results of an experimental investigation conducted to study the flexural response of RC beams strengthened using externally bonded steel-FRCM composite. Steel-FRCM composite strips were bonded to the tension face of four RC beams, which were tested in four-point bending. Parameters varied were the presence/absence of the external (coating) layer of matrix, presence/absence of U-wrap anchorages, and loading rate. The strengthened beam load responses are presented and compared, and the contribution of the composite to the flexural strength is examined. Debonding of the steel-FRCM composite strips is also discussed. Results are compared with those from single-lap direct-shear tests conducted on the same composite.

2. Experimental campaign

2.1. Material properties

The concrete beams and prisms were constructed with normal weight concrete with Portland cement (Type 1) without admixtures. The concrete water-cement ratio was 0.44, and the maximum aggregate size was 25 mm. The beams and prisms were cast from the same batch of concrete. The average compressive strength [14] and splitting tensile strength [15] determined at 28 days from six (3 + 3) 100 mm × 200 mm concrete cylinders were 31.5 MPa (CoV = 0.023) and 3.1 MPa (CoV = 0.046), respectively, and values are summarized in Table 1.

Reinforcing bars in the beam specimens were No. 3 (dia. = 9.5 mm, area = 71 mm^2) and No. 5 (dia. = 15.9 mm, area = 199 mm^2) ASTM A615 Grade 420 deformed steel bars [16]. All reinforcing bars of the same size were from the same heat. Tension tests were conducted on three samples of each bar size to determine the mechanical properties. The measured yield strength f_y and ultimate strength f_u of the No. 3 bars were 454 MPa (CoV = 0.015) and 716 MPa (CoV = 0.003), respectively. For the No. 5 bars, the measured values of f_y and f_u were 469 MPa (CoV = 0.011) and 740 MPa (CoV = 0.011), respectively.

The composite material consisted of steel fibers and a cementitious matrix. The steel fibers were produced in the form of a sheet that consisted of unidirectional twisted steel wire cords. Each cord included five filaments, three of which were straight, and the remaining two were wound around the other three at a high twist angle. The weight of fibers was 2000 g/m^2, the cord density was 0.472 cords/mm, and the cross-sectional area of each cord was 0.538 mm^2. The tensile strength, ultimate strain, and elastic modulus of the fibers reported by the manufacturer [17] were 3000 MPa, 1.5%, and 205 GPa, respectively. The matrix employed in this study, which was designed to attain high bond with the steel fibers, was an inorganic, thixotropic mineral mortar. The compressive strength and tensile strength of the matrix given by the manufacturer [17] are summarized in Table 1.

Table 1
Material properties of matrix and concrete.

	f_c (MPa)	f_t (MPa)	f_r (MPa)
Matrix	>50[a]	–	>9[a]
Concrete	31.5 (CoV = 0.023)	3.1 (CoV = 0.046)	–

Note: f_c = average compressive strength at 28 days; f_t = average splitting tensile strength at 28 days; f_r = average flexural strength at 28 days.
[a] Value reported by the manufacturer [17].

2.2. Direct-shear tests

Seven specimens presented in this paper were tested using the single-lap (direct) shear test set-up. The composite strips were externally bonded to concrete blocks (prisms). The push-pull configuration was adopted where the concrete prism was pulled while the fibers were restrained [18] (Fig. 1). The concrete prisms had a cross section b = 125 mm width × h = 125 mm depth and length L = 375 mm. Only the three faces of the prisms cast directly against the formwork were used to bond the composite strips; the face of each prism that was troweled smooth after casting was disregarded.

The concrete blocks were sandblasted prior to applying the first (internal) layer of matrix. The target roughness profile was 5 mm in accordance with the composite manufacturer's recommendation [17]. The roughness depth was measured at several discrete locations to ensure the requirements were met. Per the manufacturer's instructions [17], the concrete surface was thoroughly wetted before applying the composite. The matrix was applied only to the bonded area to embed the fibers and bond the composite to the concrete substrate (Fig. 1a). The composite was bonded starting at a distance d = 38 mm from the prism edge at the loaded end (Fig. 1a). The matrix was applied from the edge of the external longitudinal cord on one side of the fiber strip to the edge of the external longitudinal cord on the other side of the fiber strip. Fibers were bare outside the bonded area. A 4 mm thick layer of matrix (internal layer) was applied to the concrete using molds to control the composite width and thickness. A single layer of steel fibers was applied onto the internal matrix layer, and the fibers were pressed onto the matrix to maintain their alignment and assure proper impregnation by the matrix. The fiber strip was positioned such that it extended slightly beyond the end of the matrix at the free end of the composite strip as shown in Fig. 2. A second (external) 4 mm thick layer of matrix was applied over the steel fibers. The thickness of the composite strip t = 8 mm was in accordance with the manufacturer's recommendations [17]. Several specimens were cast with the external matrix layer omitted. For these specimens, after applying the fiber strip to the internal matrix layer a thin (i.e., less than 1 mm) layer of matrix was applied over the strip only to cover the fibers, and then the excess material was scraped off at the level of the fiber strip backing to minimize the amount of material on top of the fibers.

The bonded width b_1 of each composite strip was 50 mm (with n = 24 longitudinal fiber cords), and the bonded length ℓ was 330 mm. The bonded length was based on results of preliminary direct-shear tests of the same composite that indicated that the bonded length selected was longer than the effective bond length (i.e., the length over which the stress transfer zone is fully established) because a plateau was reached in the load response, as has been observed in the case of FRP-concrete joints [19,20]. Table 2 lists the direct-shear test specimens. Specimens are named following the notation DS_K_X_Y_(L_)Z, where DS indicates that the specimen was tested in single-lap direct-shear, K is used to identify the specific composite in this paper, X = bonded length (ℓ) in mm, Y = bonded width (b_1) in mm, L (if present) indicates the external layer of matrix was omitted, and Z = specimen number.

Steel plates were attached to the end of the steel fiber strip with a thermosetting epoxy resin to grip the bare steel cords during testing (Fig. 1). The plates were also bolted together with four through-bolts at the plate corners to assure a uniform pressure on the gripped fibers and to prevent slippage within the plates. The concrete prism was restrained against movement by a steel frame bolted to the testing machine base. The steel frame was made with flat bars of width w_s = 48 mm and thickness t_s = 9 mm. A 9 mm thick steel plate was inserted between the steel frame and

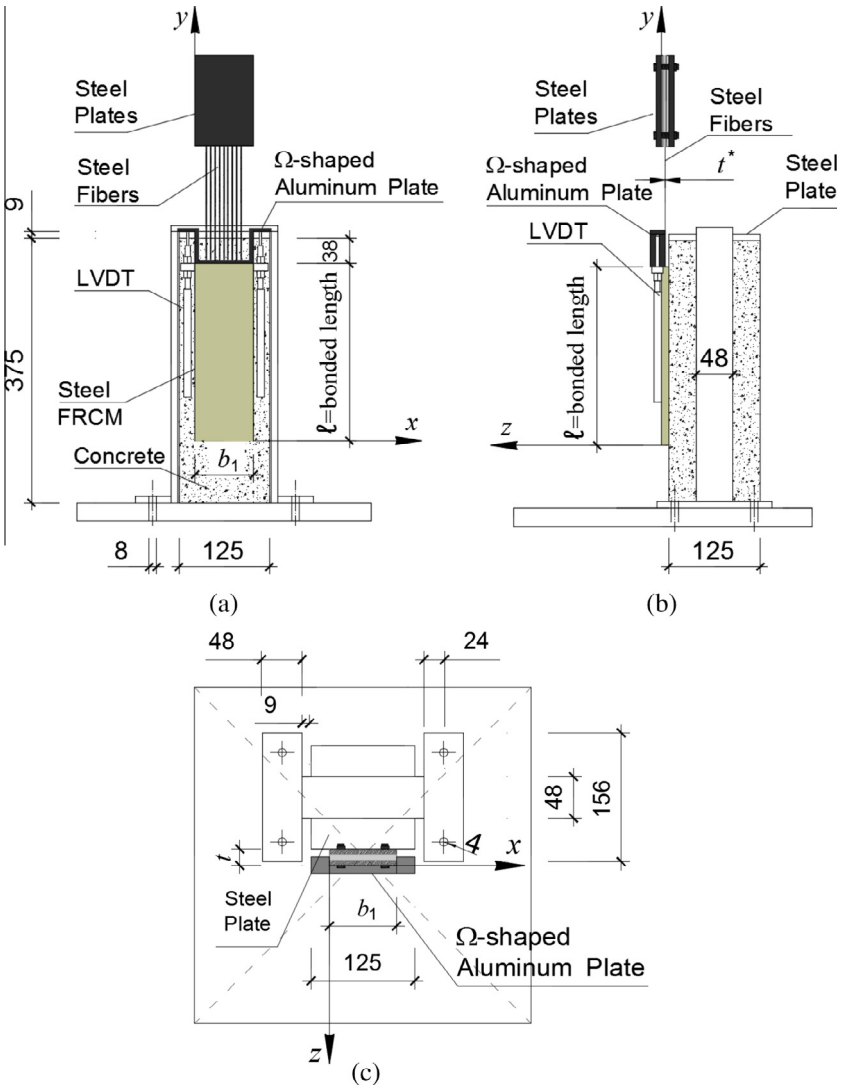

Fig. 1. Single-lap direct-shear test set-up (a) front view, (b) side view, and (c) top view (dimensions in mm).

the top of the prism to distribute the pressure provided by the frame restraint to the concrete prism (Fig. 1).

Tests were conducted under displacement control using a close-loop servo-hydraulic universal testing machine. The global slip g (i.e., slip of the fibers relative to the substrate measured at the loaded end of the composite) was increased at a constant rate of 0.00084 mm/s until failure. This rate was used in previous tests of FRCM-concrete joints by the authors [18,21,22]. Global slip was measured using two linear variable displacement transducers (LVDTs) that were attached to the concrete surface near the edge of the bonded area at the loaded end. The LVDTs reacted off of a thin aluminum Ω-shaped bent plate that was attached to the surface of the steel fibers adjacent to the beginning of the bonded area as shown in Fig. 1. The average of the two LVDT measurements, i.e., the global slip g, was used to control the displacement rate.

2.3. Beam tests

Five RC beam specimens presented in this paper had the same nominal dimensions and internal reinforcement. The beams were B = 203 mm wide, H = 305 mm deep, and L_b = 3048 mm long. Longitudinal reinforcement was comprised of two No. 5 bars (dia. = 15.9 mm) on the flexural tension side and two No. 3 (dia. = 9.5 mm) bars on the flexural compression side. Transverse reinforcing bars were No. 3 bars (dia. = 9.5 mm). The clear cover to the transverse reinforcing bars was 19 mm on all sides. Fig. 3a shows the geometry and internal reinforcement conditions.

All beams were cast in steel formwork from the same concrete batch on the same date. The beams were covered with wet burlap for 28 days, after which they remained in the laboratory until they were tested.

Four beams were strengthened, and one unstrengthened beam served as the control (reference) beam. The control beam was named B_Control. The strengthened beams were named following the notation B_K_(L_ or U_)XV, where B indicates beam specimen, K is used to identify the specific composite in this paper, L (if present) indicates the external layer of matrix was omitted, U (if present) indicates that U-wraps were provided at the ends of the composite strip, and XV indicates the loading rate, where X is the multiplier on the base loading rate V = 0.013 mm/s; X = 1 or 2 corresponds to a loading rate of 0.013 mm/s or 0.025 mm/s, respectively. The beam specimens are listed in Table 3. The different test parameters are further discussed in the paragraphs that follow.

Three of the four strengthened beams (beams B_K_1V, B_K_2V, and B_K_L_1V) were strengthened prior to loading. The steel-FRCM composite strengthening system was applied to the three beams

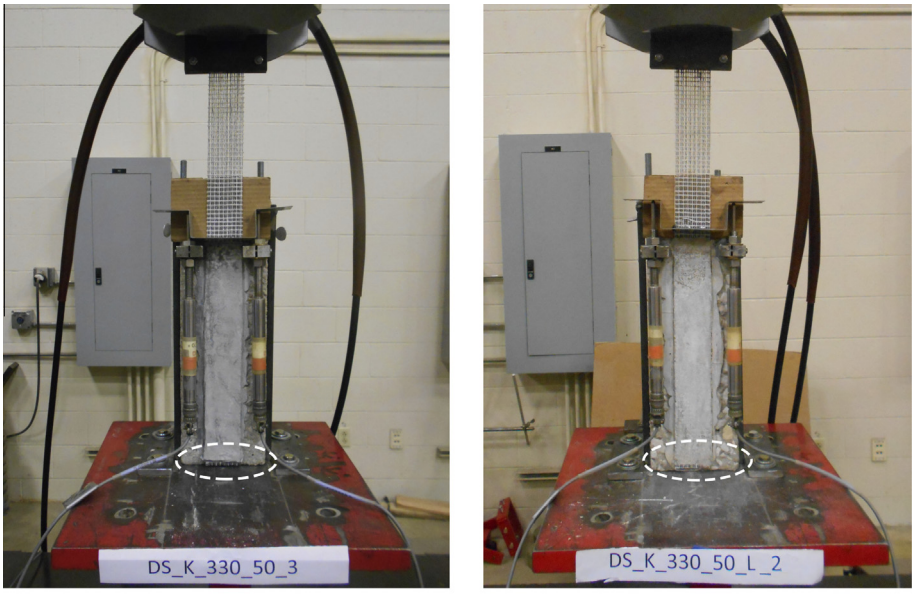

Fig. 2. Photo of single-lap direct-shear test (a) specimen with external matrix layer (specimen DS_K_330_50_3 shown) and (b) specimen with the external matrix layer omitted (specimen DS_K_330_50_L_2 shown). Note the fibers extending beyond the bonded area at the free end (circled in the photographs).

Table 2
Steel-FRCM single-lap direct-shear test specimens.

Specimen	Composite width b_1 (mm)	Composite length ℓ (mm)	Number of fiber cords n	Maximum load P^* (kN)	Ultimate stress σ^* (MPa)
DS_K_330_50_1	50	330	24	9.48	734
DS_K_330_50_3	50	330	24	8.57	664
DS_K_330_50_4	50	330	24	8.80	682
DS_K_330_50_L_1	50	330	24	8.07	625
DS_K_330_50_L_2	50	330	24	9.64	747
DS_K_330_50_L_3	50	330	24	9.92	768
DS_K_330_50_L_4	50	330	24	9.45	732

Note: Specimen DS_K_330_50_2 is not included because of problems during testing.

on the same day, 28 days after the concrete was cast. The fourth strengthened beam (beam B_K_U_1V) was part of a different test series (not reported in this paper). During the initial test it was loaded to approximately 90% of the yield load of the control beam (using the same test set-up as the other beams), then it was subsequently unloaded and strengthened as part of this test series. Flexural cracks occurred in the concrete beam during the initial test, but no significant residual deflection was present after the initial test. The composite strengthening system of beam B_K_U_1V was applied approximately three months after the concrete was cast.

The steel-FRCM composite was applied to the flexural tension surface of the beams following the same procedure used to apply the composite for the direct-shear specimens (Section 2.2). Photographs of the installation procedure are shown in Fig. 4. The concrete was sandblasted with a target roughness profile of 5 mm (Fig. 4a). The roughness depth was measured at several discrete locations to ensure the requirements were met. Per the manufacturer's instructions [17], the concrete surface was thoroughly wetted before applying the composite. The matrix was applied from the edge of the external longitudinal cord on one side of the fiber strip to the edge of the external longitudinal cord on the other side of the fiber strip. A 4 mm thick layer of matrix (internal layer) was applied to the concrete using molds to control the composite width and thickness. A single layer of steel fibers was applied onto the internal matrix layer, and the fibers were pressed onto the matrix to maintain their alignment and assure proper impregnation by the matrix. A second (external) 4 mm thick layer of matrix was applied over the steel fibers. The composite sheet was 153 mm wide (with n = 72 longitudinal fiber cords) and 2210 mm long for all strengthened beams. U-wraps made of the same composite were installed at ends of the composite on the preloaded strengthened beam (beam B_K_U_1V) using the same procedure described above. The width of the U-wraps was 250 mm (Fig. 3b) and was designed considering test results presented in [13]. The thickness t of the composite was 8 mm in all cases. The composite was covered in wet burlap until the test date, which was 28–32 days after casting the composite. The steel-FRCM layout is illustrated in Fig. 3b.

Each specimen was instrumented with a combination of sensors to measure force, displacement, and internal reinforcement strain at key locations. All devices were connected to a data acquisition system controlled by a personal computer. The applied load was measured by a load cell within the hydraulic actuators. Displacement was measured at five locations along the length of each beam using six LVDTs. Displacement measurements were taken at the supports (one at each support), at the applied loads (one at each point load), and at mid-span (one each side of the beam; two total). Eight uniaxial electric resistance strain gages were applied to the longitudinal reinforcing bars in the tension and compression regions within the constant moment region of the beam. The instrumentation layout is shown in Fig. 3c.

The beams were tested in four-point bending under quasi-static loading conditions. The span length ℓ_b was 2438 mm. The load was

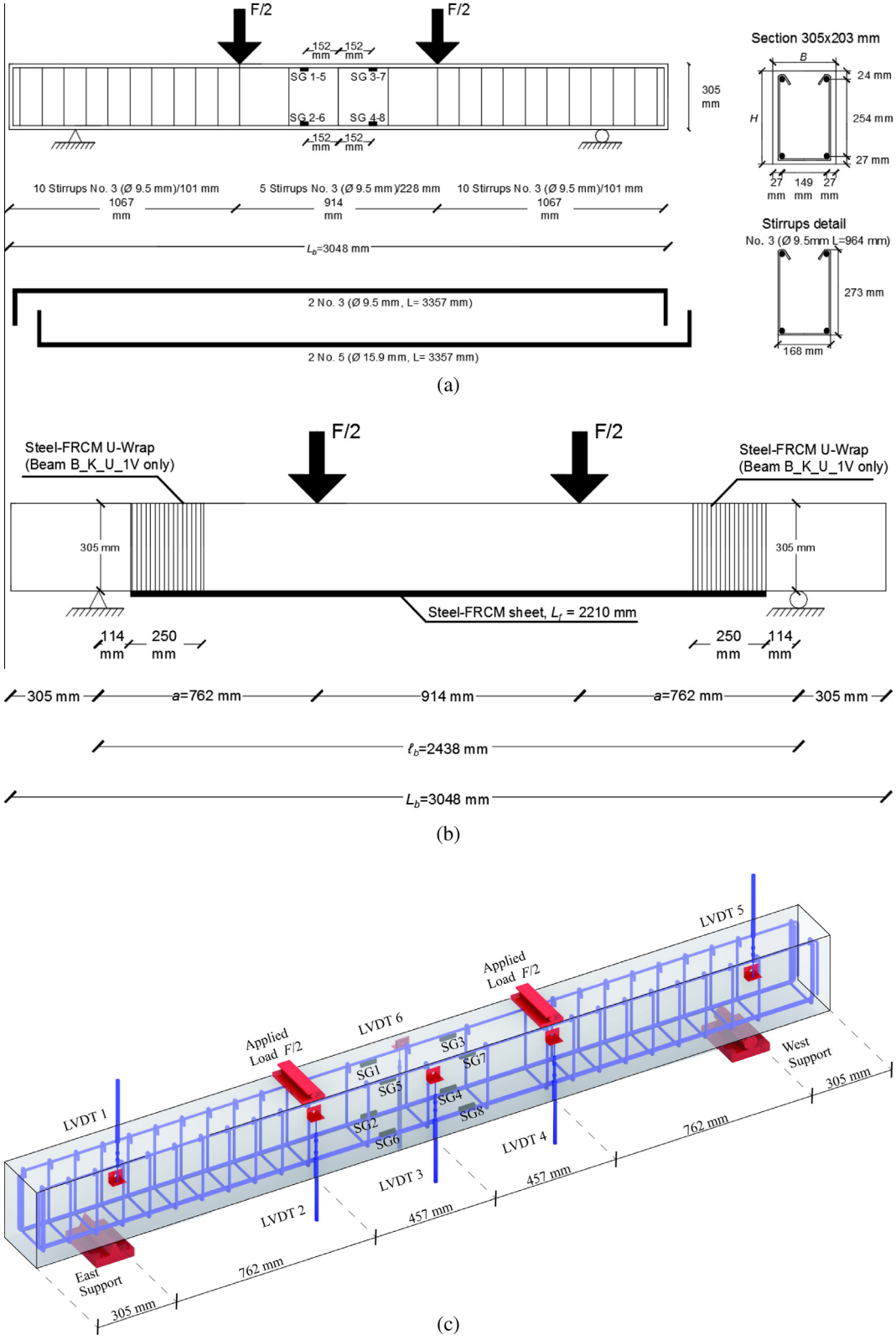

Fig. 3. Beam geometry and reinforcement: (a) reinforcing steel layout, (b) steel-FRCM layout, and (c) instrumentation layout.

applied to the beam specimens by two closed-loop servo hydraulic actuators, each with a capacity of 490 kN, that were suspended from a steel loading frame. The two actuators were attached to the ends of a stiff steel beam affixed to the top middle of, and oriented orthogonal to, a stiff steel spreader beam. The spreader beam distributed the load to the test beam in two locations. The beams were loaded under displacement control by controlling the average displacement of the two actuators. The unstrengthened beam (beam B-Control) was loaded at a load rate of 0.013 mm/s. Three of the strengthened beams were tested with a load rate of

Table 3
Beam test specimens.

Specimen	F_{cr} (kN)	F_y (kN)	F_{deb} (kN)	$\left(\frac{F_y}{F_{y,control\ beam}}\right)$	$\left(\frac{F_{deb}}{F_y}\right)$	Δ_{cr} (mm)	Δ_y (mm)	Δ_{deb} (mm)	$\left(\frac{\Delta_{deb}}{\Delta_y}\right)$	Failure mode
B_Control	43.37	135.55	–	–	–	2.50	13.09	–	–	(2)
B_K_1V	44.57	156.02	177.75	1.15	1.14	1.57	11.31	20.25	1.79	Debonding
B_K_2V	45.44	161.98	189.06	1.19	1.17	2.04	12.10	23.12	1.91	Debonding
B_K_L_1V	48.33	164.55	195.81	1.21	1.19	1.67	10.80	22.37	2.07	Debonding
B_K_U_1V	NA(1)	159.74	177.88	1.18	1.11	NA(1)	11.08	18.98	1.71	Debonding

Notes:
1. Not available; beam was cracked prior to testing.
2. Not available; beam was not tested to failure.

Fig. 4. Photos of beam specimen preparation: (a) concrete surface, (b) fibers being applied to internal matrix layer, and (c) external matrix layer.

0.013 mm/s, and one was tested with a load rate of 0.025 mm/s to examine whether varying the load rate caused a significant difference in results. The control beam was loaded in two stages, where the first stage proceeded from zero to a point on the yield plateau, at which point the applied load was released to zero. Then the load was reapplied, and loading progressed until the end of the test. The four strengthened beams were loaded in three stages. The first stage proceeded from zero until a point on the response beyond the first yielding load, at which point the applied load was released to zero. The load was then reapplied and progressed until immediately after debonding of the composite occurred, at which point the applied load was again released to zero. Finally, the load was reapplied, and loading progressed until the end of the test. After each stage, the loading process was temporarily paused and held constant to document the observations and take photographs during testing. All beams were tested beyond their yield load and debonding load (where applicable), but only one beam (B_K_U_1V) was tested to failure because the other beams were to be repaired in a separate study.

3. Experimental results

3.1. Single-lap direct-shear tests

3.1.1. General behavior and failure mode

All single-lap shear test specimens, with and without the external matrix layer (the DS_K_330_50 and DS_K_330_50_L series, respectively), failed due to composite debonding. Failure was characterized by a sudden and brittle detachment of the fiber strip and external matrix layer (if present). For all specimens, the interfacial crack formed along the fibers (Fig. 5a). Debonding occurred at the internal matrix-fiber interface and was the result of fracture of the matrix in between the fibers. Fig. 5b shows a representative photo of the DS_K_330_50 series specimens after failure. Interlaminar failure (delamination) of the matrix has also been reported for other types of FRCM composites [22], in addition to slippage of the fibers from the embedding matrix [18,21], detachment of the composite strip at the FRCM-concrete interface [23], or fiber fracture [24]. These results suggest that the failure mode is dependent on the characteristics of the composite and concrete substrate and the mechanical and fracture properties of the different materials at different interfaces.

For specimens with the steel-FRCM composite strip and with the external layer of matrix (DS_K_330_50 series), increasing global slip resulted in the formation of transversal hairline cracks in the matrix (Fig. 5c). The first crack generally formed near the composite loaded end, then additional cracks formed progressively towards the composite free end with increasing global slip. The cracks were visible on the external surface of the composite and appeared to extend from the external surface to the steel fiber strip. This cracking can be explained as when the interfacial shear stresses increase, slippage of the fibers at the internal matrix layer interface occurs. Since the external matrix layer is bonded to the fibers, it translates with the slipped fibers. Thus, cracking of the external matrix layer occurs due to compatibility as the fibers and the external layer of matrix slip relative to the internal matrix layer, which is bonded to the concrete substrate.

3.1.2. Applied load – global slip response

Fig. 6 shows the applied load P – global slip g response of the single-lap shear specimens. The load responses are also shown in terms of stress σ, where σ is defined in Eq. (1):

$$\sigma = \frac{P}{nA^*} \tag{1}$$

in which P is the load applied to the composite by the testing machine, n is the number of longitudinal fiber cords (24), and A^* is the area of each cord (0.538 mm^2).

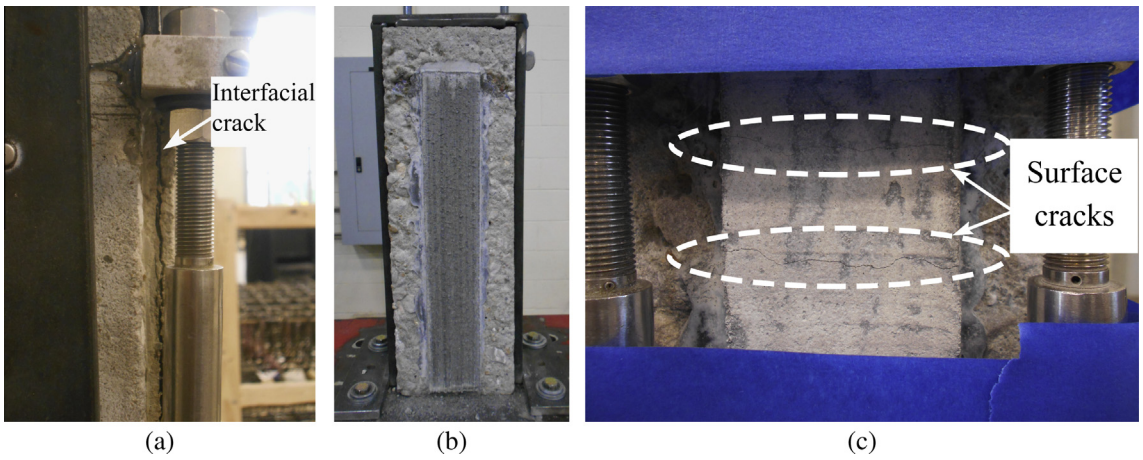

Fig. 5. Photos of single-lap shear test specimens: (a) crack along interface of cords and matrix, (b) surface of internal matrix layer after failure (specimen DS_K_330_50_1 shown), and (c) cracking observed on surface of external matrix layer.

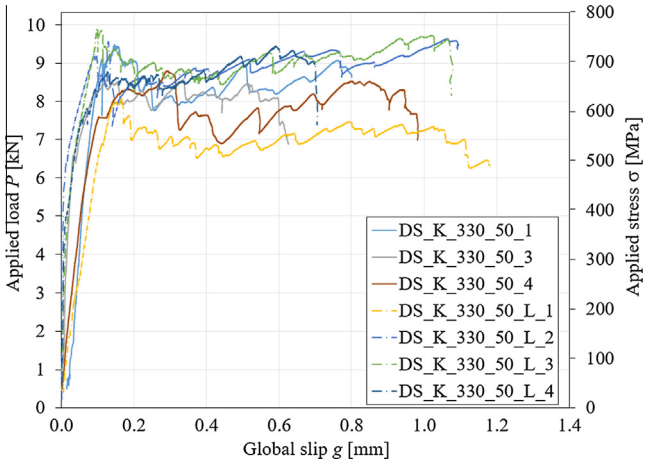

Fig. 6. Applied load P – global slip g response and applied stress σ – global slip g response of single-lap direct-shear specimens.

The graphs in Fig. 6 show that the load responses of specimens with and without the external matrix layer are similar. The experimental evidence suggests that the initial part of the load response is represented by a linear branch associated with elastic behavior of the bond between the fibers and the matrix. Following, a slight reduction in stiffness occurs where the interface between the steel fibers and the matrix experiences some microdamage. After the maximum load P^* is reached, further increases in global slip generally result in a near-constant applied load until a sudden and rapid degradation of load occurs with no distinct softening response.

The maximum load P^* is reported in Table 2 for each specimen. Table 2 also includes the ultimate stress σ^*, i.e., the stress at maximum load P^*, where stress σ is defined in Eq. (1). The average value of σ^* for the DS_K_330_50 series was 693 MPa, and the average value of σ^* for the DS_K_330_50_L series was 718 MPa. The average value considering all specimens $\bar{\sigma}^*$ was 707 MPa.

It should be noted that for the case of FRP-concrete joints, it has been shown that the interfacial crack initiates in the non-linear, pre-peak region of the response, then unstable crack growth results in the sharp drop in load immediately after the peak load is achieved [19]. Accordingly, the value of P^* may overestimate the load corresponding to steady propagation of the interfacial crack for specimens with bonded length longer than the effective bond length.

3.2. Beam tests

3.2.1. General behavior and failure mode

The unstrengthened beam (B_Control) exhibited the typical flexural behavior of a flexure-dominated, underreinforced RC beam, with the gradual occurrence and progression of flexural and flexure-shear cracks and a significant amount of deflection.

For the strengthened beams without U-wrap anchorages (beams B_K_1V, B_K_2V, and B_K_L_1V), flexural cracks first appeared within the constant moment region and progressed in length and number with increasing load. Flexural and flexure-shear cracks also appeared within the shear span regions on each end of the beam. The cracks in the concrete beam extended through the thickness of the matrix and were observed on the external surface of the composite. Interfacial cracks formed within the composite at the level of the fibers in the constant moment region at the localized locations of flexural cracks as shown in Fig. 7a. The failure mode of each beam, shown in Fig. 8, was associated with a sudden and rapid progression of interfacial cracking near the support at one end of the composite resulting in peel-off of the external matrix layer and fibers. This failure mode is consistent with the failure mode observed in the studies by Napoli and Realfonzo [12] and Prota et al. [3,7] on beams strengthened in flexure with steel-FRCM composite without anchorage. Debonding occurred at the fiber-internal matrix layer, similar to the single-lap direct-shear tests. In some cases, portions of the internal matrix layer and concrete substrate at the flexural crack locations were still attached to the external matrix layer and fibers after failure (see Fig. 8b and c). Even with video footage, it was not possible to determine whether failure initiated within the constant moment region or at the composite end because of the rapid and brittle nature of the debonding.

For beam B_K_U_1V, which had U-wrap anchorages at the ends of the composite strip, the flexural and flexure-shear cracking behavior was similar to that of the strengthened beams without U-wrap anchorages. The cracks in the concrete beam extended through the thickness of the matrix and were observed on the external surface of the composite. Although the presence of interfacial cracks near the ends of the composite could not be physically observed due to the presence of the U-wraps, interfacial cracks were observed within the composite at the level of the fibers at the toes of flexural cracks in the constant moment region (see Fig. 7b), which coalesced and progressed rapidly towards the support and underneath the U-wrap resulting in slippage of the composite strip from beneath the U-wrap (see Fig. 7c and d). This

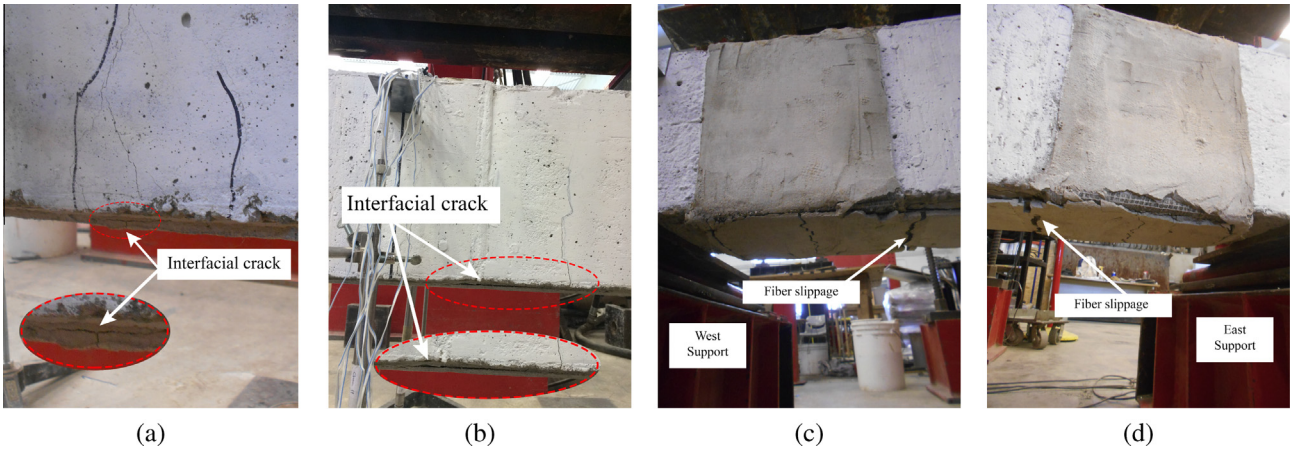

Fig. 7. Interfacial crack in beam constant moment region of (a) B_K_1V and (b) B_K_U_1V; Fiber slippage of beam B_K_U_1V after failure at (c) west U-wrap and (d) east U-wrap.

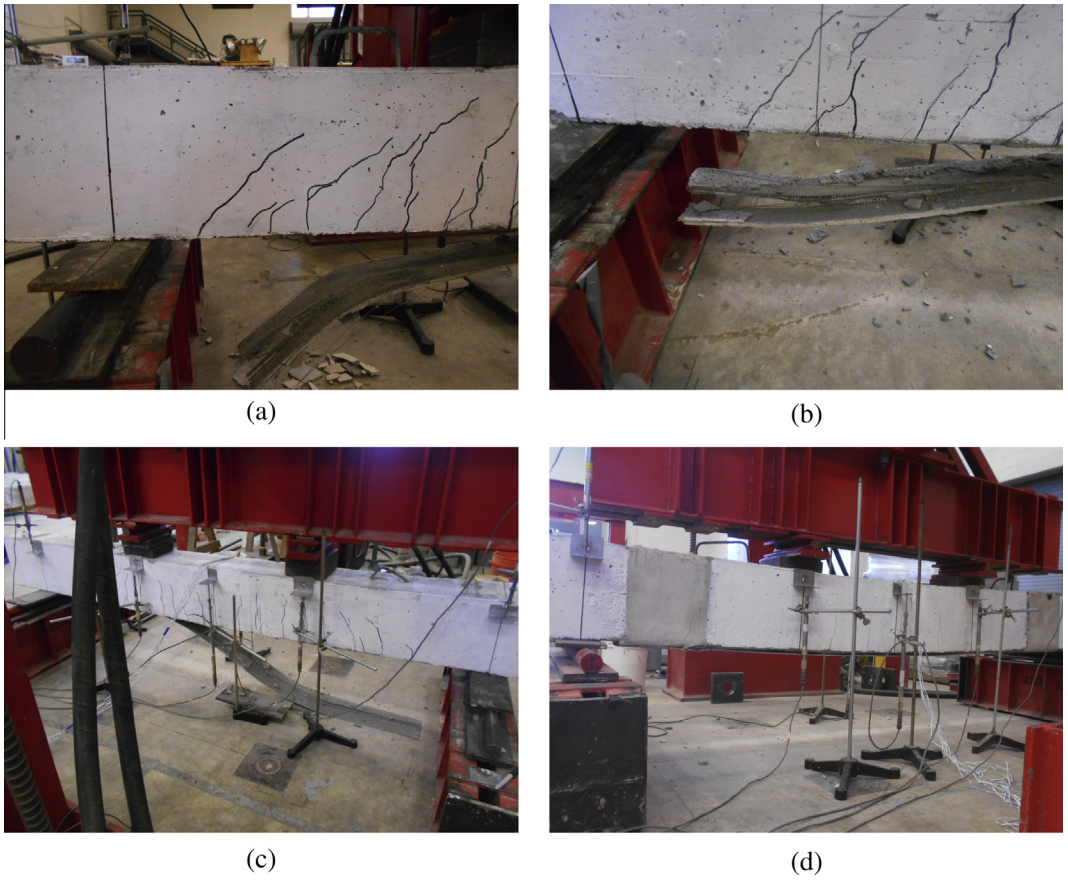

Fig. 8. Photos of beam failure modes (a) B_K_1V, (b) B_K_2V, (c) B_K_L_1V, and (d) B_K_U_1V.

slippage is consistent with observations reported by Prota et al. [3,7] on beams strengthened in flexure with steel-FRCM with anchorage (nail anchors). Further increases in displacement resulted in additional slippage of the fibers beneath both U-wraps, shown in Fig. 7c and d, with no increase in applied load because the composite was not effectively anchored at the ends. No detachment or fiber rupture of the U-wrap side faces was observed, even after significant slippage of the composite (Fig. 7c and d). Further discussion on the failure mode is included in Section 4.2.1.

Final crack patterns for each beam are shown in Fig. 9. The number and distribution of flexural and flexure-shear cracks were similar for the unstrengthened and strengthened beams, with and without U-wraps.

3.2.2. Applied load - displacement response

The total applied load F - midspan displacement Δ response for each beam is shown in Fig. 10. The term F is used to denote the applied load for the beam tests, where F is the sum of the two point loads (see Fig. 3). Table 3 summarizes key points in the load

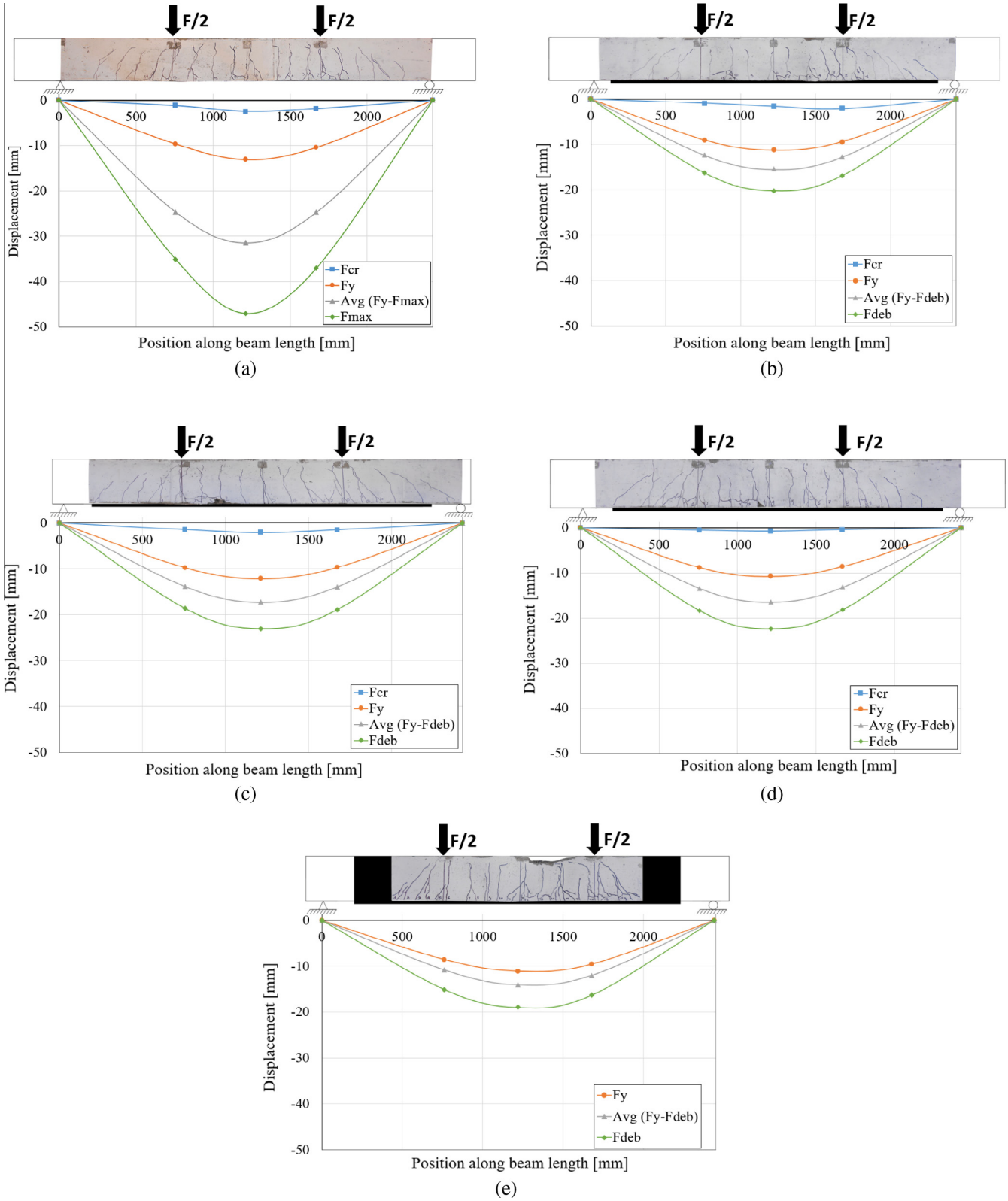

Fig. 9. Measured displacement along the length at different load levels and final crack patterns (a) B_Control, (b) B_K_1V, (c) B_K_2V, (d) B_K_L_1V, and (e) B_K_U_1V.

response, including the applied load F_{cr} associated with cracking, the applied load F_y associated with first yielding of the tensile steel reinforcing bars (indicated by a change in slope in the graph and confirmed with strain gage measurements), and the applied load F_{deb} at which debonding of the composite occurred. Corresponding midspan displacement values Δ_{cr}, Δ_y, and Δ_{deb} are also reported in Table 3.

The unstrengthened beam B_Control exhibited a change in stiffness at applied load F = 43.37 kN, associated with flexural cracking, and again at F = 135.55 kN, associated with first yielding of the

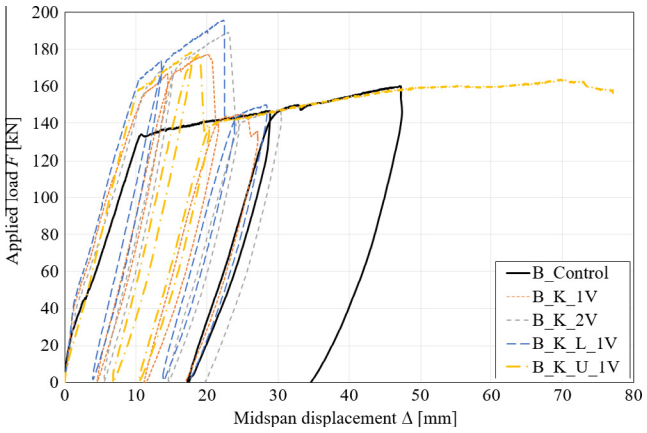

Fig. 10. Applied load F – midspan displacement Δ response of beam specimens.

flexural tension reinforcement. As expected, the strengthened beams had a similar cracking load and a slightly larger initial stiffness and post-cracking stiffness as compared to the control beam. For all strengthened beams, debonding of the composite strip was associated with a rapid reduction in applied load, after which the load response followed the load response of the unstrengthened beam.

Fig. 9 shows the displacement measured by the LVDTs (accounting for the displacements measured at the supports) along the beam length at different load levels. Values of displacement reported at midspan are the average of the two LVDT measurements at that location. Locations of LVDTs and measured values are indicated by markers in the graphs. For beam B_Control, values are shown at load levels corresponding to cracking F_{cr}, yielding F_y, the maximum applied load F_{max}, and an intermediate point halfway between F_y and F_{max}. For each of the strengthened beams, values are shown at load levels corresponding to cracking F_{cr}, yielding F_y, the load at which debonding occurred F_{deb}, and an intermediate point halfway between F_y and F_{deb} for the corresponding beam.

3.2.3. Strain measurements

The applied load F versus axial strain measured in the reinforcing steel bars is shown in Fig. 11 for each beam. Readings from strain gages that malfunctioned are not shown. Strain gage positions are denoted in Fig. 3c. The strain measurements are used to determine the moment-curvature response and estimate the strain in the composite at debonding in Section 4.2.2 of this paper.

4. Analysis and discussion

4.1. Single-lap direct-shear tests

In general, the applied load P – global slip g responses of the steel-FRCM composite-concrete joints shown in Fig. 6 resemble those of FRP-concrete joints reported in the literature [19,20]. The plateau in the load response suggests that the load-carrying capacity of the interface was achieved, and therefore the bonded length was longer than the effective bond length [18,21]. However, determination of the value of the effective bond length requires further study.

The load response of the steel-FRCM composite is different from that of other FRCM composite-concrete joints with PBO, glass, or carbon fibers reported in the literature [21,22] in several respects. For each composite mentioned above, failure is located at the fiber-matrix interface, however in the case of other FRCM composites debonding has been shown to be characterized by significant slippage of the fibers relative to the matrix. Accordingly for the case of PBO, glass, or carbon FRCM composites, when the composite bonded length is longer than the effective bond length, a post-peak load softening response is observed with a non-zero load at the end of the response associated with friction that is due to interlocking among fibers and between fibers and matrix [21]. On the other hand, for the steel-FRCM composite tested in this study, the global slip was relatively small at the initiation of debonding (on the order of 1/10 that of PBO-FRCM composite, for example [21]), and failure was associated with fiber slippage and fracture of the matrix in the plane of the fibers. This response resulted in complete detachment of the external matrix layer and fiber strip with no softening response (Fig. 6). More work is needed to study the stress transfer mechanism and determine whether friction (interlocking) between fibers and matrix plays a role in the load response, as is the case with other FRCM composites reported in the literature [21].

Table 2 and Fig. 6 show that the peak load (peak stress) and load response of the specimens with the steel-FRCM composite with the external layer of matrix omitted (DS_K_330_50_L series) is nearly the same as specimens with the external matrix layer included (DS_K_330_50 series); in fact, the average peak stress of specimens without the external matrix layer is approximately 4% larger than the average peak stress of specimens with the external matrix layer, even with a non-contrasted Mode I (peeling) loading condition [25]. This result suggests that the external matrix layer does not play a significant role in the stress transfer mechanism for this composite, which can be explained by the fact that the failure mode observed, i.e., fiber slippage and interlaminar matrix fracture, is dominated by a Mode-II (shear) condition. The average peak stress of specimens with and without the external matrix layer were 24.8% and 25.6%, respectively, of the tensile strength of fibers reported by the manufacturer [17].

4.2. Beam tests

4.2.1. Effectiveness of strengthening system

The effectiveness of the strengthening system in the beam tests is examined in terms of stiffness, yield load, and debonding load and corresponding midspan displacement. As expected, Fig. 10 shows that the post-cracking stiffness of strengthened beams B_K_1V, B_K_2V, and B_K_L_1V was slightly larger than that of the unstrengthened control beam. Beam B_K_U_1V, which was pre-cracked prior to testing, had an initial stiffness similar to the post-cracking stiffness of the other strengthened beams. Table 3 summarizes the increase in the yield load for each strengthened beam relative to that of the control beam $F_y/F_{y,control\ beam}$. The strengthening system increased the yield load by 15–21% relative to the unstrengthened beam. Values of F_y for each of the strengthened beams were very close since the steel fiber density was the same for each beam. The load at which debonding occurred F_{deb} was larger than the yield load F_y for each strengthened beam, and Table 3 shows that the ratio F_{deb}/F_y ranged from 1.11 to 1.19. The ratio of the midspan displacement at debonding to that at yielding Δ_{deb}/Δ_y, i.e., the displacement ductility of the strengthened beams, ranged from 1.71 to 2.07. Although the control beam was not tested to failure, the load responses in Fig. 10 show that the ductility of the strengthened beams was lower than that of the control beam.

Fig. 10 and Table 3 show that the initial stiffness, yield load, and debonding load and corresponding midspan displacement of beam B_K_L_1V, with the external matrix layer omitted, were similar to the strengthened beams with the external matrix layer (B_K_1V and B_K_2V). This suggests that the external matrix layer does not improve the effectiveness of the strengthening system. Furthermore, the failure load and failure mode were similar for specimens with and without the external matrix layer, which implies

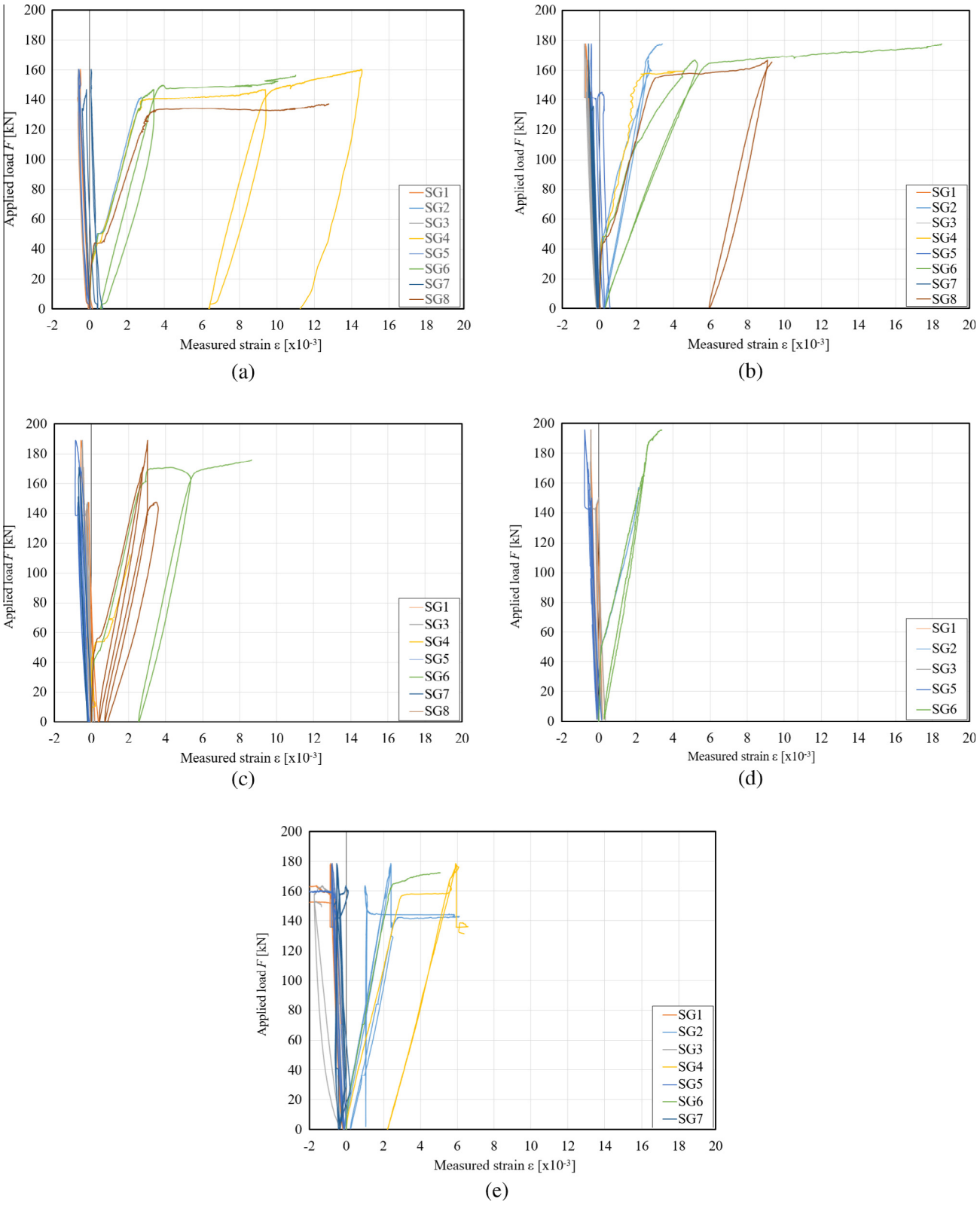

Fig. 11. Applied load *F* versus reinforcing steel bar strain response (malfunctioning gages not shown). (a) B_Control, (b) B_K_1V, (c) B_K_2V, (d) B_K_L_1V, and (e) B_K_U_1V.

that the external matrix layer does not play a role in mitigating composite debonding, as discussed in Section 4.1 for the direct-shear tests. In fact, debonding of beam B_K_L_1V occurred at a load and midspan displacement that were slightly larger than those of beams B_K_1V and B_K_2V, which may be because the composite without the external matrix layer had a lower bending stiffness [26]. It is possible that the lower stiffness allowed for better composite action because of delayed failure.

The initial stiffness, yield load, debonding load and corresponding midspan displacement, and failure mode of beam B_K_2V,

which had a load rate that was twice that of the other beam specimens, were similar to those of beam B_K_1V. These results suggest that the load rates employed did not significantly affect the failure mode or the load and midspan displacement at debonding. However, more work is needed to study the potential effects of load rate on the bond behavior and stress transfer of FRCM composites.

It is interesting to note that the debonding load and corresponding midspan displacement for beam B_K_U_1V, with U-wraps anchorages, were similar to those of the strengthened beams without U-wraps (B_K_1V, B_K_2V, and B_K_L_1V), which indicates that the U-wraps did not improve the effectiveness of the strengthening system. Based on the behavior of beam B_K_U_1V discussed in Section 3.2.1, it appears that the U-wraps helped to restrain the composite peel-off that occurred in the strengthened beams without the U-wraps, however, they did not restrain the fiber-matrix interfacial slip at the composite ends. These results suggest that a mix of debonding phenomena (i.e., a combination of Mode II [shear] and Mode I [peeling] loading conditions) occurred at different locations along the bonded length that contributed to the failure mechanism.

The observation regarding lack of effectiveness of the U-wraps in this study is also significant because it suggests that some traditional types of anchorages [27,28] used to anchor the ends of FRP composites might not be effective for FRCM composites. As noted by Grelle and Sneed [28], several traditional types of anchorages used to mitigate plate end debonding [29] in FRP do so by restraining the out-of-plane peeling effect, which is significant in the case of FRP-concrete joints where debonding occurs within the concrete substrate immediately beneath the composite. On the other hand, such anchorages are generally not effective in restraining slippage of the fibers at the fiber-matrix interface, which governs the failure of certain FRCM composite-concrete joints [21]. Lack of anchorage effectiveness was also noted by Prota et al. [3], who used nail anchors in an attempt to improve the performance of externally bonded steel-FRCM for flexural strengthening of RC beams. Accordingly, an effective anchorage for FRCM composites must be capable of restraining the fiber slippage. Further work is needed to study this issue.

4.2.2. Strains in the composite

Strains in the composite were not measured directly, but the maximum axial strain in the fibers at composite debonding $\varepsilon_{f,max}$ was estimated using three different methods. In Method 1, the strains measured in the reinforcing steel bars (Fig. 11), along with the assumptions that cross-sections remain plane (Bernoulli) and perfect bond between the concrete and composite and reinforcing bars up to failure, were used to estimate the strain in the composite at the debonding load. The strain gages were located in the constant moment region (see Fig. 3c).

In Method 2, the contribution of the composite strengthening system to the bending moment capacity was used to estimate the strain in the composite using Eq. (2) [30]:

$$\varepsilon_{f,\max} = \frac{\Delta M}{0.9HE_f nA^*} \tag{2}$$

where ΔM is the contribution of the composite to the moment at debonding, H is the height of the beam, E_f is the modulus of elasticity of the fibers, n is the number of longitudinal fiber cords, and A^* is the area of the cord. ΔM was determined as the increase in moment corresponding to debonding of the strengthened beam relative to that of the control beam determined at same level of deflection (Fig. 10). The factor 0.9 in the denominator of Eq. (2) is used to approximate the internal moment arm of the composite at failure (assumed $0.9H$).

In Method 3, moment-curvature analysis was carried out to predict the cross-sectional response of the strengthened beam. Results in [13] show that the experimental load response of RC beams strengthened in flexure with FRCM composites can be reasonably predicted using this simple analytical model. In the analysis, the reinforcing steel bars were assumed to be elastic-perfectly plastic with a yield strength corresponding to the material tests. The steel-FRCM composite was assumed to be linear-elastic with properties given by the manufacturer [17]. Two different stress-strain relations for concrete given by Hognestad [31] and EC2 [32] were used, each with a peak value of compressive and tensile stress corresponding to those measured in the concrete material tests (Section 2.1). The corresponding results are referred to as Moment-curvature 1 and 2, respectively. The moment at debonding (corresponding to F_{deb}) in the constant moment region was used to determine the corresponding strain in the composite. As noted in [13], values of fiber strain determined in this manner are a gross approximation of the debonding strain but are meaningful if it is assumed that debonding is related only to the fiber strain local value.

Table 4 summarizes values of $\varepsilon_{f,max}$ determined using the three methods described above. Average values of $\varepsilon_{f,max}$ determined using strain profiles, Eq. (2), and moment-curvature analysis are 0.54%, 0.73%, and 0.83%, respectively. Fig. 12 compares the tensile stress in the fibers at debonding, where the tensile stress was obtained by multiplying the strain by the modulus of the fibers. It should be noted that the maximum strains and stresses in Table 4 and Fig. 12 are computed for the maximum moment along the beam length, which occurs in the constant moment region. Values of the fiber strength reported by the manufacturer [17] and the average value of ultimate stress from all single-lap direct-shear tests $\bar{\sigma}^*$ (reported in Table 2) are also shown in Fig. 12 for comparison. The corresponding average value of strain from the direct shear tests $\bar{\varepsilon}^* = \bar{\sigma}^*/E_f$ is 0.34%.

Values of $\varepsilon_{f,max}$ in Table 4 and fiber tensile stress in Fig. 12 computed by using moment-curvature analysis are similar (within 1% on average) with slight differences due to the concrete constitutive relationships employed. Values computed using the approximate method of Eq. (2) are generally consistent with those determined by moment-curvature analysis (within 10% on average), with differences in part due to the approximation in the internal moment arm of the composite at failure. Values computed using the strain profiles are generally lower than corresponding values determined by the other methods (by at least 25%). The source of this difference can be explained by the fact that strain gage readings can be erroneous near the location of a major crack, and also once debonding of the composite has initiated. Fig. 11 shows significant variability in the reinforcing bar strain measurements (especially in the tension reinforcement), and certain gages malfunctioned when they were located at or near a concrete crack. Similar irregularities would also be expected in the steel-FRCM composite due to extension of flexural cracks through the matrix resulting in irregular strain profiles. As previously discussed, while the assumption of plane cross-sections, including the strengthening material, globally allows for good prediction of the results [13], local effects are not considered. Because of these issues and the fact that the strain profiles were determined from a limited number of functioning gages, the values of $\varepsilon_{f,max}$ determined herein using this method should be viewed more qualitatively than quantitatively.

Results in Fig. 12 show that the maximum tensile stress in the fibers determined using the three methods was less than the fiber tensile strength, which is consistent with the fact that fiber rupture was not observed. As expected, results also show that the maximum tensile stress in the fibers in the beam tests was larger than the ultimate stress $\bar{\sigma}^*$ of the single-lap direct-shear tests, where

Table 4
Maximum strain in the composite at debonding.

Specimen	Method 1 (strain profile) $\varepsilon_{f,max}$ $\times 10^{-6}$	Method 2 (Eq. (2)) $\varepsilon_{f,max}$ $\times 10^{-6}$	Method 3 (moment-curvature 1[a]) $\varepsilon_{f,max}$ $\times 10^{-6}$	Method 3 (moment-curvature 2[b]) $\varepsilon_{f,max}$ $\times 10^{-6}$
B_K_1V	4255	6200	7323	7380
B_K_2V	7258	7749	8089	8141
B_K_L_1V	4293	9051	10,575	10,619
B_K_U_1V	5637	6367	7097	7141
Average	5361	7342	8271	8320

Notes:
[a] Concrete stress-strain relationship by Hognestad [31].
[b] Concrete stress-strain relationship by EC2 [32].

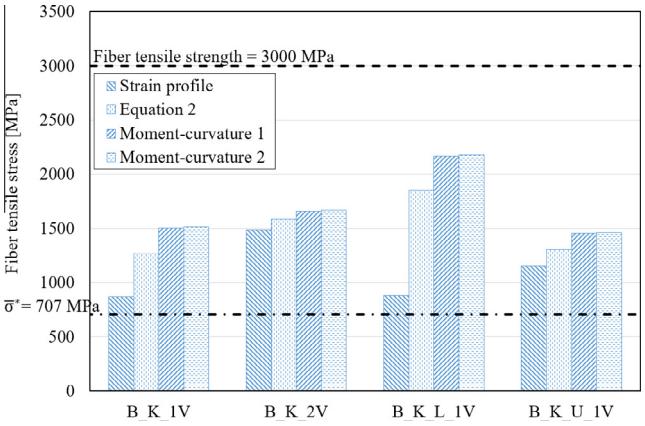

Fig. 12. Comparison of stress in fibers at failure determined using strain profiles, Eq. (2), and moment-curvature analysis (1: Hognestad [31]; 2: EC2 [32] stress-strain relationship for concrete).

the peak stress in the direct-shear test is the result of a load (stress) applied to the composite in one direction [33].

5. Conclusions

This paper presented the results of an experimental investigation conducted to study the flexural response of reinforced concrete (RC) beams strengthened using externally bonded steel fiber reinforced cementitious matrix (steel-FRCM) composites. The results of five beam specimens were presented, and results were compared with those of single-lap direct-shear tests of the same composite. The following conclusions are made based on the findings of this study:

1. Debonding of the steel-FRCM joints tested in single-lap direct-shear tests was characterized by fiber slippage and fracture of the matrix layer at the internal matrix layer-fiber interface. Unlike with other FRCM-concrete joints reported in the literature (i.e., PBO-, glass-, carbon-FRCM), the load response of the bonded composite exhibited no post-peak softening response.
2. RC beams strengthened in flexure with steel-FRCM composite failed due to loss of composite action from debonding of the composite. Debonding occurred at the fiber-internal matrix layer, similar to the single-lap direct-shear tests. Failure of the strengthened beams without U-wraps was associated with a sudden, rapid progression of interfacial cracking resulting in peel-off of the external matrix layer and fibers. For the strengthened beam with U-wraps, the evidence suggests that a mix of debonding phenomena (i.e., a combination of Mode II [shear] and Mode I [peeling] loading conditions) occurred at different locations along the bonded length that contributed to the failure mechanism.
3. The strengthening system increased the yield load by 15–21% relative to the unstrengthened beam. The debonding load was larger than the yield load, and the ratio of the load at which debonding occurred to the load at yielding F_{deb}/F_y ranged from 1.11 to 1.19 for each strengthened beam. The ratio of the midspan displacement at debonding to that at yielding Δ_{deb}/Δ_y ranged from 1.71 to 2.07.
4. The load rate employed and the presence of the external matrix layer did not appear to have a significant effect on the failure mode or the load and midspan displacement at debonding. However, more work is needed to study the potential effects of load rate on the bond behavior and stress transfer of FRCM composites.
5. The debonding load and corresponding midspan displacement for the strengthened beam with U-wraps anchorages were similar to those of the strengthened beams without U-wraps, which indicates that the U-wraps did not improve the effectiveness of the strengthening system. The presence of U-wraps helped to restrain the peel-off of the composite observed in strengthened beams without the U-wraps; however, they did not restrain the fiber-matrix interfacial slip that inhibited composite action for beam B_K_U_1V. This observation is significant because it suggests that some of the traditional types of anchorages used to anchor FRP composites might not be effective for FRCM composites. Further work is needed to study this issue.
6. Average values of the maximum fiber strain at debonding $\varepsilon_{f,max}$ determined using strain profiles, Eq. (2), and moment-curvature analysis were 0.54%, 0.73%, and 0.83%, respectively. These values were less than the fiber rupture strain of 1.5% and were larger than the average value determined from the direct-shear tests of 0.34%.

Acknowledgements

The experimental work discussed in this paper was conducted at Missouri University of Science and Technology (Missouri S&T). The authors would like to express their appreciation to Kerakoll S.p.A. of Sassuolo, Italy, who provided the composite materials in this study.

References

[1] ACI Committee 440. Guide for the design and construction of externally bonded FRP systems for strengthening concrete structures (ACI 440.2R-08). Farmington Hills, MI: American Concrete Institute; 2008.
[2] Wobbe E, Silva P, Barton BL, Dharani LR, Birman V, Nanni A, et al. Flexural capacity of R/C beams externally bonded with SRP and SRG. In: Proc of society for the advancement of material and process engineering symp, Long Beach, CA, USA. p. 20–7.
[3] Prota A, Manfredi G, Nanni A, Cosenza E, Pecce M. Flexural strengthening of R/C beams using emerging materials: ultimate behavior. In: Proc of CICE, Adelaide, Australia. p. 163–70.

[4] Kim JY, Fam A, Kong A, El-Hacha R. Flexural strengthening of RC beams using steel reinforced polymer (SRP) composites. In: Proc of the 7th int symp FRP reinforcement for concrete structures, ACI SP-230, 1, paper #93. p. 1647–64.
[5] Barton B, Wobbe E, Dharani LR, Silva P, Birman V, Nanni A, et al. Characterization of reinforced concrete beams strengthened by steel reinforced polymer and grout (SRP and SRG) composites. Mater Sci Eng A 2005;412(1–2):129–36.
[6] Casadei P, Nanni A, Alkhrdaji T, Thomas J. Performance of double-t prestressed concrete beams strengthened with steel reinforced polymer. Adv Struct Eng 2005;8(4):427–42.
[7] Prota A, Tan KY, Nanni A, Pecce M, Manfredi G. Performance of shallow R/C beams with externally bonded steel-reinforced polymer. ACI Struct J 2006;103 (2):163–70.
[8] Pecce M, Ceroni F, Prota A, Manfredi G. Response prediction of R/C beams externally bonded with steel reinforced polymers. J Compos Constr 2006;103 (2):195–203.
[9] Ceroni F, Pecce M. Cracking behaviour of RC beams externally strengthened with emerging materials. Constr Build Mater 2007;21:736–45.
[10] Balsamo A, Nardone F, Iovinella I, Ceroni F, Pecce M. Flexural strengthening of concrete beams with EB-FRP, SRP and SRCM: experimental investigation. Composites B 2013;46:91–101.
[11] Hawileh R, Abdalla J, Nawaz W, Alzeer A, Muwafi R, Faridi A. Strengthening reinforced concrete beams in flexure using hardwire steel fiber sheets. In: Proc of CICE, Vancouver, Canada, August 20–22. p. 22.
[12] Napoli A, Realfonzo R. Reinforced concrete beams strengthened with SRP/SRG systems: experimental investigation. Const Build Mater 2015;93:654–77.
[13] D'Ambrisi A, Focacci F. Flexural strengthening of RC beams with cement-based composites. J Compos Constr 2011;15(5):707–20.
[14] ASTM C39. Standard test method for compressive strength of concrete cylinder specimens. West Conshohocken, PA: ASTM; 2016. p. 7.
[15] ASTM C496. Standard test method for splitting tensile strength of cylindrical concrete specimens. Conshohocken, PA: ASTM; 2011. p. 5.
[16] ASTM A615. Standard specification for deformed and plain carbon-steel bars for concrete reinforcement. West Conshohocken, PA: ASTM; 2015. p. 8.
[17] Kerakoll S.p.A. – web site: <www.kerakoll.com>; 2016 [accessed Feb 2016].
[18] Sneed LH, D'Antino T, Carloni C. Investigation of bond behavior of PBO fiber-reinforced cementitious matrix composite-concrete interface. ACI Mater J 2014;111(5):569–80.
[19] Subramaniam KV, Carloni C, Nobile L. An understanding of the width effect in FRP–concrete debonding. Strain 2011;47:127–37.
[20] Carloni C, Subramaniam KV. Application of fracture mechanics to debonding of FRP from RC members. SP-286. ACI; 2012. p. 10-1–10-14.
[21] D'Antino T, Carloni C, Sneed LH, Pellegrino C. Matrix-fiber bond behavior in PBO FRCM composites: a fracture mechanics approach. Eng Fract Mech 2014;117:94–111.
[22] D'Antino T, Pellegrino C, Carloni C, Sneed LH. Experimental analysis of the bond behavior of glass, carbon, and steel FRCM composites. Key Eng Mater 2015;624:371–8.
[23] D'Antino T, Sneed LH, Carloni C, Pellegrino C. Influence of the substrate characteristics on the bond behaviour of FRCM-concrete joints. Constr Build Mater 2015;101(1):838–50.
[24] Carozzi FG, Carlo P. Mechanical properties and debonding strength of fabric reinforced cementitious matrix (FRCM) systems for masonry strengthening. Compos B Eng 2015;70(2015):215–30.
[25] D'Antino T, Sneed LH, Carloni C, Pellegrino C. Effect of the inherent eccentricity in single-lap direct shear tests of FRCM-concrete joints. Compos Struct 2016:13. http://dx.doi.org/10.1016/j.compstruct.2016.01.076.
[26] Teng JG, Smith ST, Yao J, Chen JF. Intermediate crack-induced debonding in RC beams and slabs. Constr Build Mater 2003;17(6–7):447–62.
[27] Kalfat R, Al-Mahaidi R, Smith S. Anchorage devices used to improve the performance of reinforced concrete beams retrofitted with FRP composites: state-of-the-art review. J Compos Constr 2013;17(1):14–33.
[28] Grelle SV, Sneed LH. Review of anchorage systems for externally-bonded FRP laminates. Int J Concr Struct Mater 2013;7(1):17–33.
[29] Teng JG, Chen JF, Smith ST, Lam L. FRP strengthened RC structures. West Sussex: Wiley; 2002.
[30] Carloni C, Bournas D, Carozzi G, D'Antino T, Fava G, Focacci F, et al. Fiber reinforced composites with cementitious (inorganic) matrix. In: Pellegrino C, Sena-Cruz J, editors. Design procedures for the use of composites in strengthening of reinforced concrete structures. RILEM state-of-the-art reports 19. RILEM; 2016. p. 349–91 [chapter 9].
[31] Hognestad E. Study of combined bending and axial load in reinforced concrete members. University of Illinois. Engineering Experiment Station. Bulletin; No. 399; 1951.
[32] CEN Eurocode 2. Design of concrete structures-Part 1-1: general rules and rules for buildings. prEN 1992-1-1; 2003.
[33] Rosenboom O, Rizkalla S. Modeling of IC debonding of FRP-strengthened concrete flexural members. J Compos Constr 2008;12(2):168–79.